Electronic Supplementary Material (ESI) for Catalysis Science & Technology.

Supporting Information

Scanning electron microscopy (SEM) (1/4)

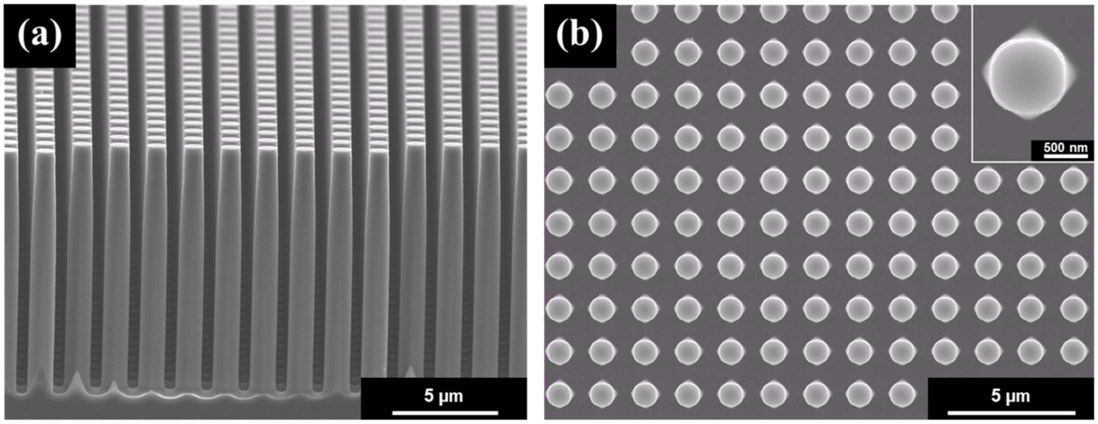

Fig. S1 SEM images of the silicon microwire array fabricated using the dry etching technique: (a) cross-section and (b) top view. The inset shows a single microwire with the ~1 µm diameter.

The silicon microwires were fabricated using the ion and dry etching technique. The wires measured 1.0 ± 0.2 µm in diameter and 10.0 ± 0.2 µm in length. The gap between the wires fabricated by oxide pattern was 0.5 ± 0.1 µm. No particles were formed on the surface or between the microwires after the HMDS vapor treatment. The silicon array morphology was preserved without any obvious changes.

SEM (2/4)

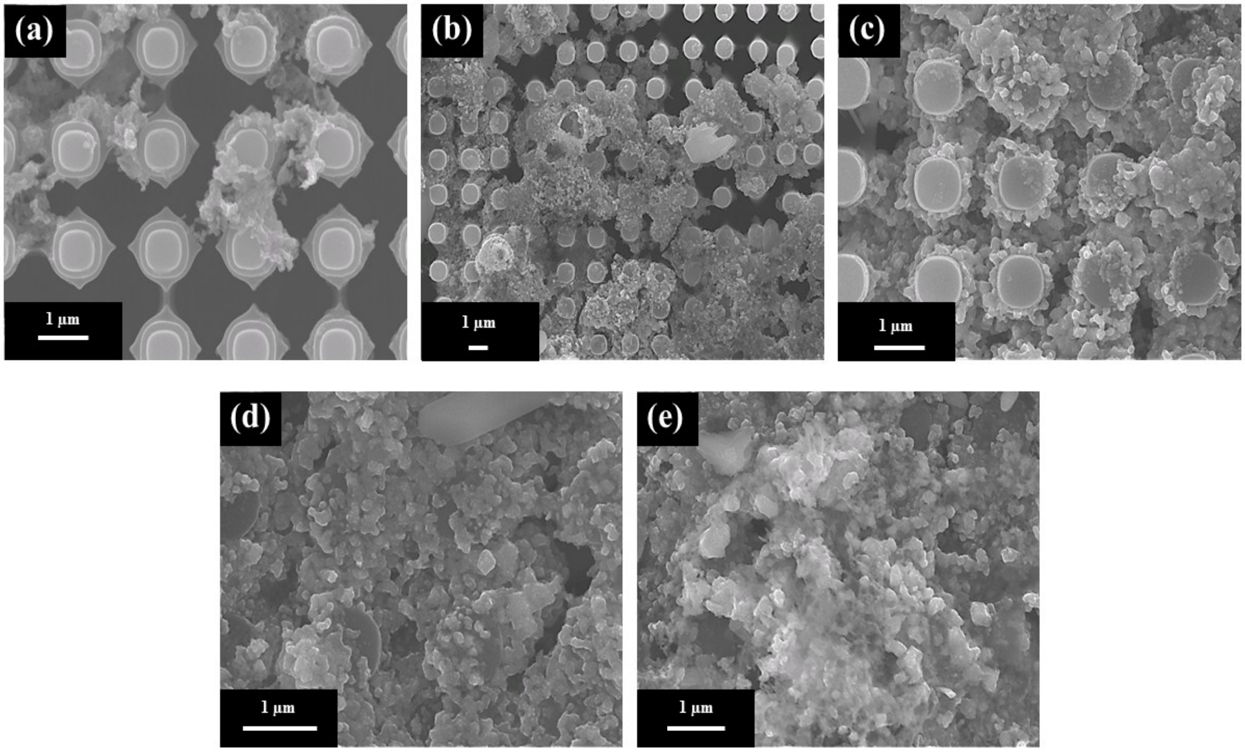

Fig. S2 Top-view of the SEM images of the silicon microwires coated by different drop-casting volumes: (a) 10, (b) 20, (c) 30, (e) 40, and (f) 50 μL of drop-casting solution.

Different volumes of the drop-casting solution were used in the silicon microwires. The amount of the drop-casting volume was related to the numbers of the microwires at the surface and the roughness factor. The optimal volume for the Si-MWs fabricated in this work according to microwire density was 30 μL for 1 × 1 cm^2 silicon microwire array. Fig. S2 shows the SEM images of the coated surface of the different drop-cast volumes of the samples. The thickness of the coated cocatalyst increased on the surface by increasing the amount of the drop-casting volume from 10 μL to 50 μL. This increase also reduced light absorbance mainly because of the aggregation of the cocatalyst particles on the array surface, which generated a reduced amount of photocarriers and led to the photocurrent loss. The SEM images also showed that different volumes led to various layer forms and particles in the silicon array, that is, from low-coated wires with some islands on the surface to the formation of a thick film on the surface that entirely covered the array surface (by increasing the volume from 10 to 50 μL). In the case of the low drop-casting volume with respect to the surface area (10 μL drop-casting volume), most of the silicon array remained uncoated. Furthermore, only some particles in the form of separated islands formed on the surface. In the case of the higher drop-casting volume subjected to the surface, the formation of a thick film on the surface (up to ~10 μm) was perceived because of the particle aggregation on the silicon surface.

SEM (3/4)

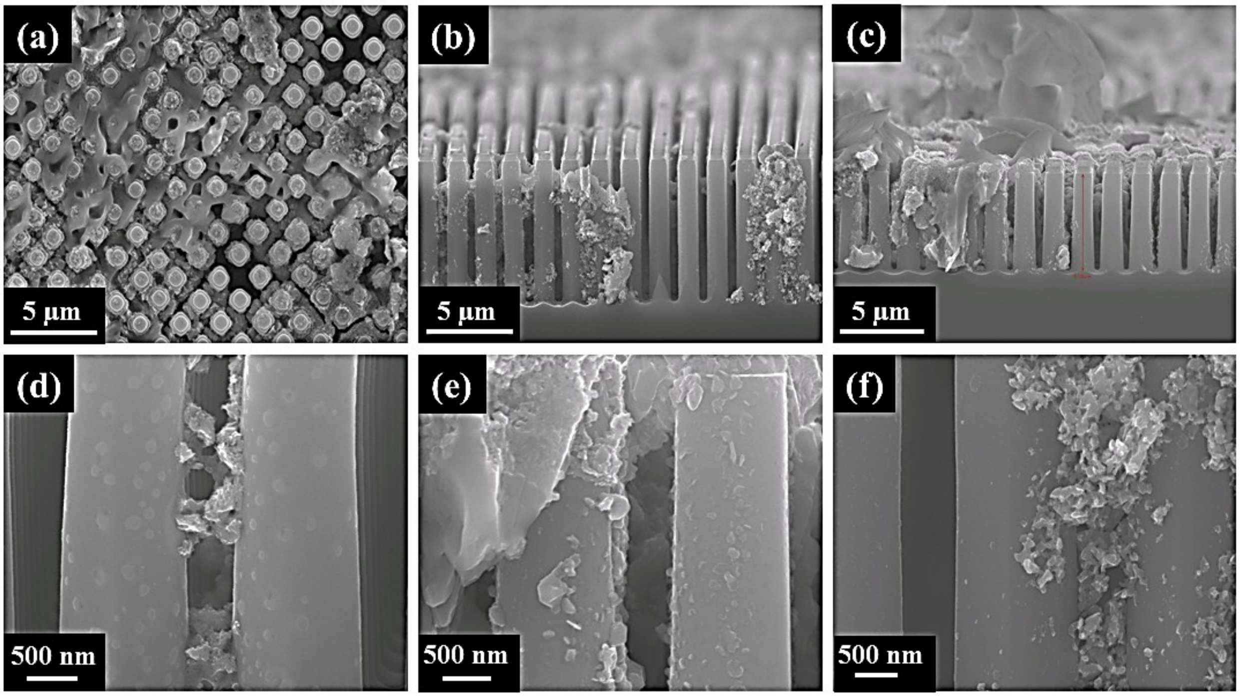

Fig. S3 SEM images of the vapor-treated silicon microwires by HMDS: (a) top-view and (b–f) cross-section after 3 h of PEC measurements[1].

SEM (4/4)

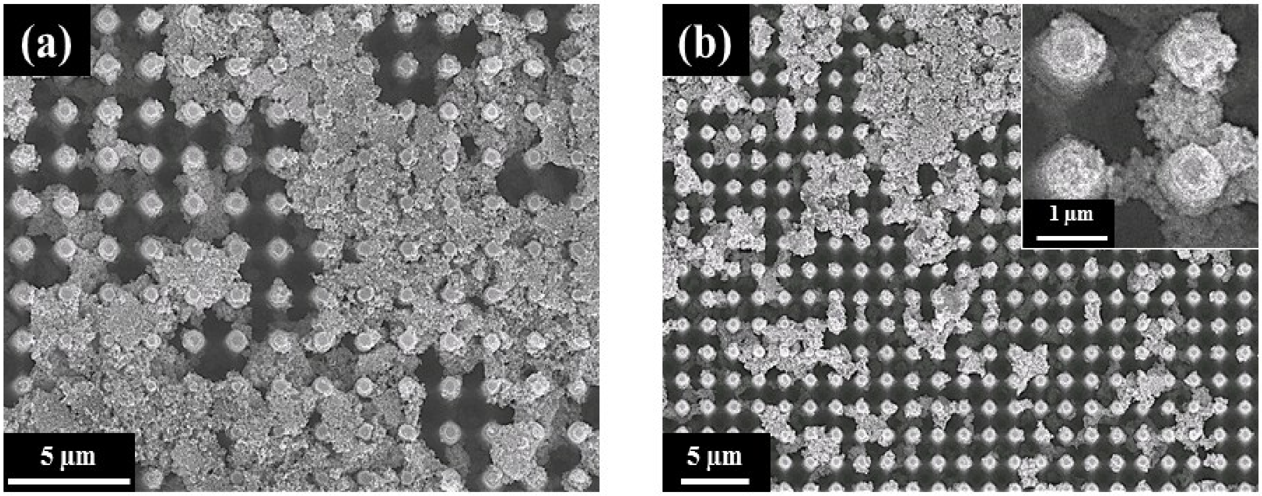

Fig. S4 Top-view SEM images of the $CoTe_2$ at TiO_2-10 nm–Si MWs array before and after the PEC tests: top view (a) before and (b) after the PEC test.

The $CoTe_2$ particles were still found on the wire surface after the PEC test, which showed the binding stability caused by the treatment of the surface with the HMDS vapor. As illustrated in Fig. S4, the particle morphology barely changed after the PEC test despite the applied voltage and evolved gas. The morphology was mostly preserved on the surface and edge of the silicon microwires. The PEC tests included three cycles of linear sweep voltammetry, 4000 s of chronoamperometry, and 3 h of hydrogen evolution reaction with two times of etching in HF (10%) interval during the reaction time (Fig. S24). The samples showed -6.3 mA cm^{-2} photocurrent density after being etched in the HF aqueous solution. A comparison with the untreated samples showed that more particles remained on the surface of the silicon microwires after the HMDS vapor treatment. This result confirmed that HMDS led to the enhanced binding of more particles onto the surface, which also enhanced the sample stability in the PEC measurements.

High-resolution transmission electron microscopy (HR-TEM)/EDAX (1/5)

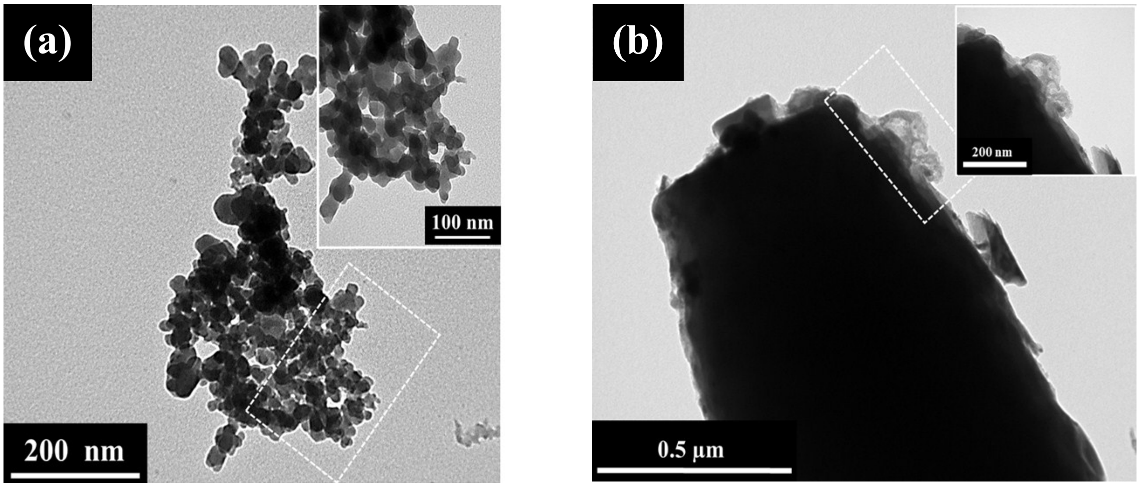

Fig. S5 TEM images of $CoTe_2$: (a) powder form (b) on the tip and surface of the silicon microwire. Inset of the selected zoomed area is shown for each figure.

The HR-TEM image of the sample in powder form (Fig. S5a) fabricated by the same drop-casting solution revealed an agglomerated particle despite 10 min of sonication in a water bath (~37 kHz), which could be related to the magnetic properties of $CoTe_2$. [1] In contrast to the severe sonication condition, the detached microwires showed the presence of particles on the tip and edge, which indicated good binding and stability of the coated samples across the wires (Fig. S5b). Observing the coated silicon wires was performed by stripping the coated microwires from the substrate by mild scratching on the surface and sonication (~37 kHz) for 5 minutes in pure ethanol (see Fig. S6).

HR-TEM/EDAX (2/5)

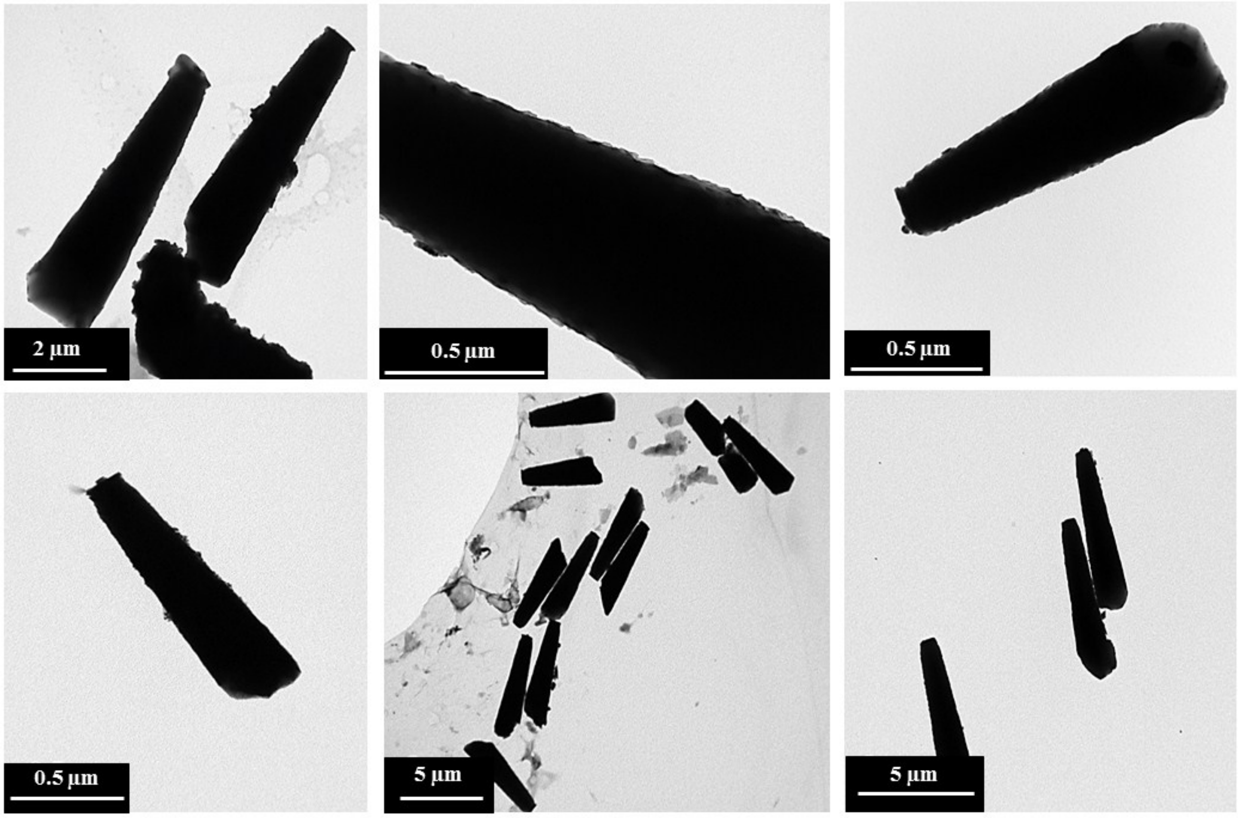

Fig. S6 TEM images of the detached silicon microwires separated by sonication from the substrate surface.

HR-TEM/EDAX (3/5)

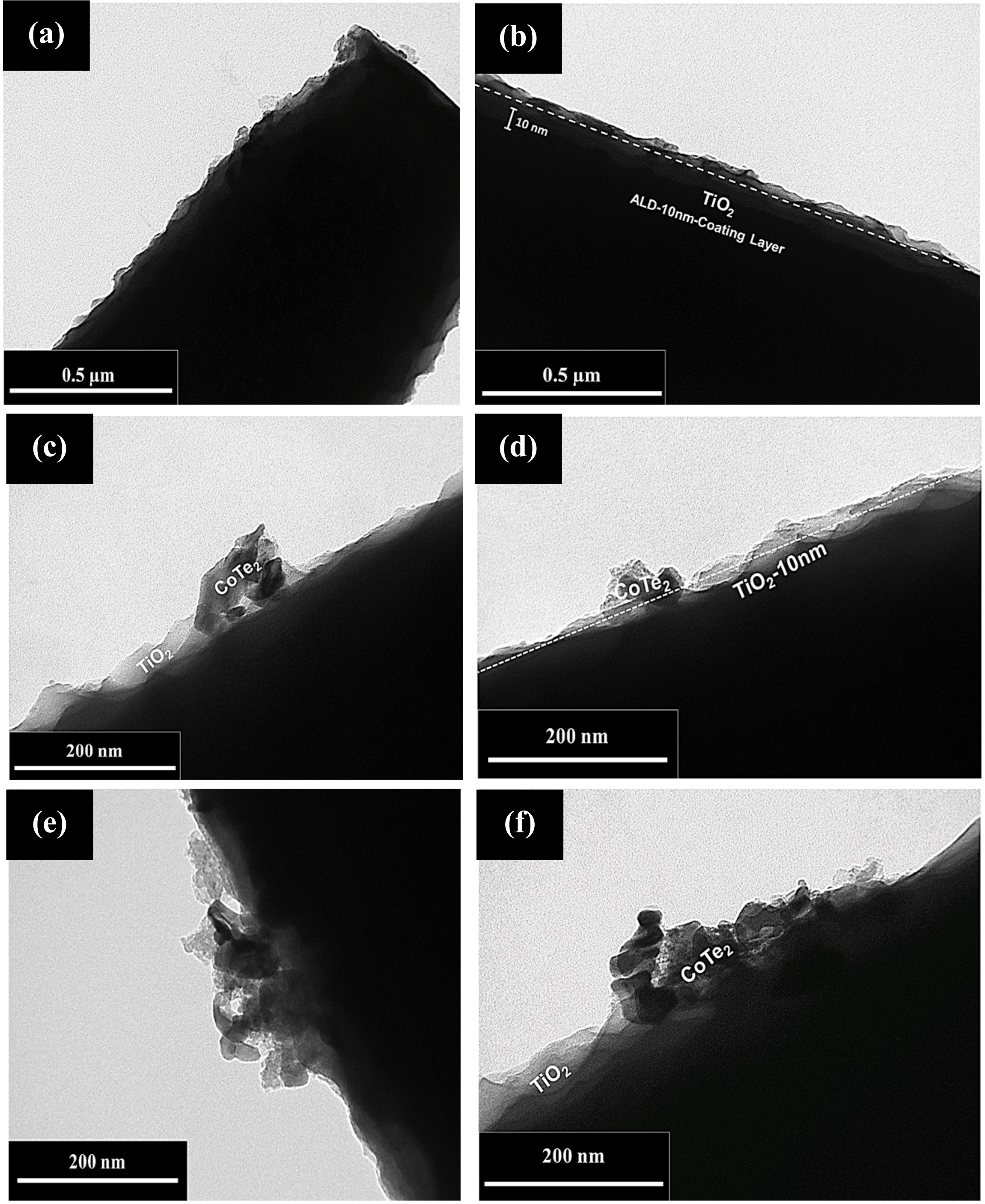

Fig. S7 TEM images of the silicon microwires: (a) tip and (b) coated microwire by nominal 10 nm-ALD; (c–f) $CoTe_2$ particles at Si-MWs with deposited ALD-10 nm–TiO_2 layer without HMDS treatment.

HR-TEM/EDAX (4/5)

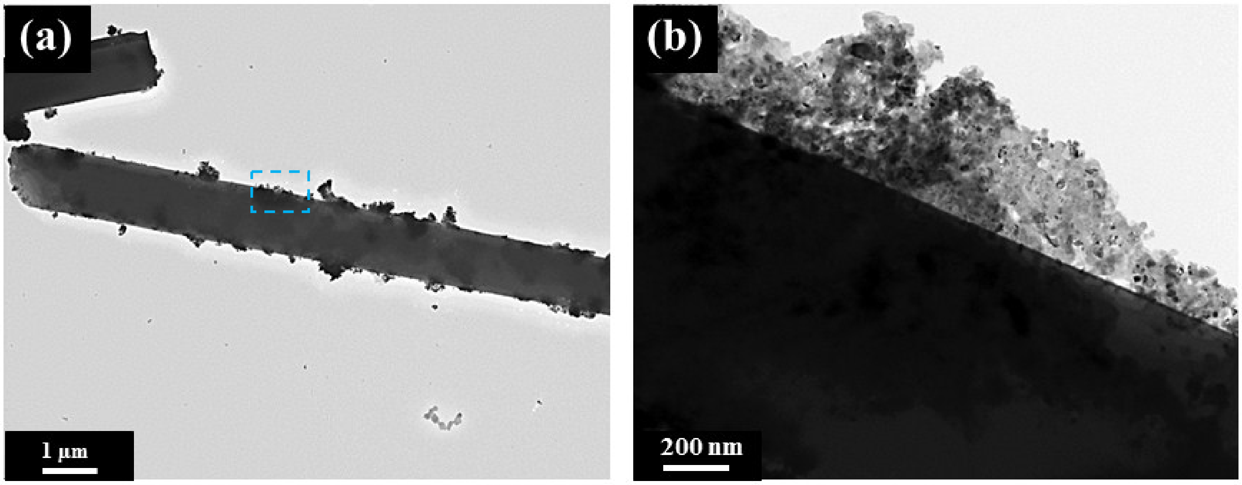

Fig. S8 TEM images of the vapor-treated silicon microwires by HMDS: (a) single wire and (b) zoom view of the selected area demonstrating a particle on the wire surface.

HR-TEM/EDAX (5/5)

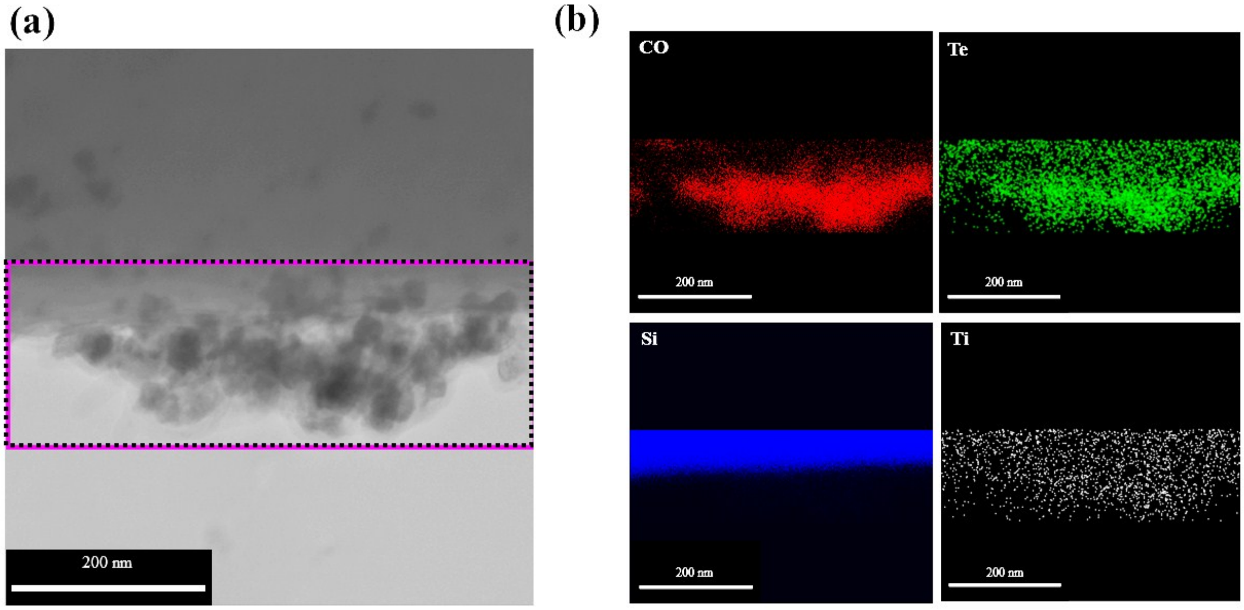

Fig. S9 HR-TEM and EDS mapping of the selected area: (a) HR-TEM image of the $CoTe_2$ particles on the silicon wire surface and (b) EDS elemental mapping of cobalt (*red*), tellurium (*green*), titanium (*white*), and silicon (*blue*) microwires.

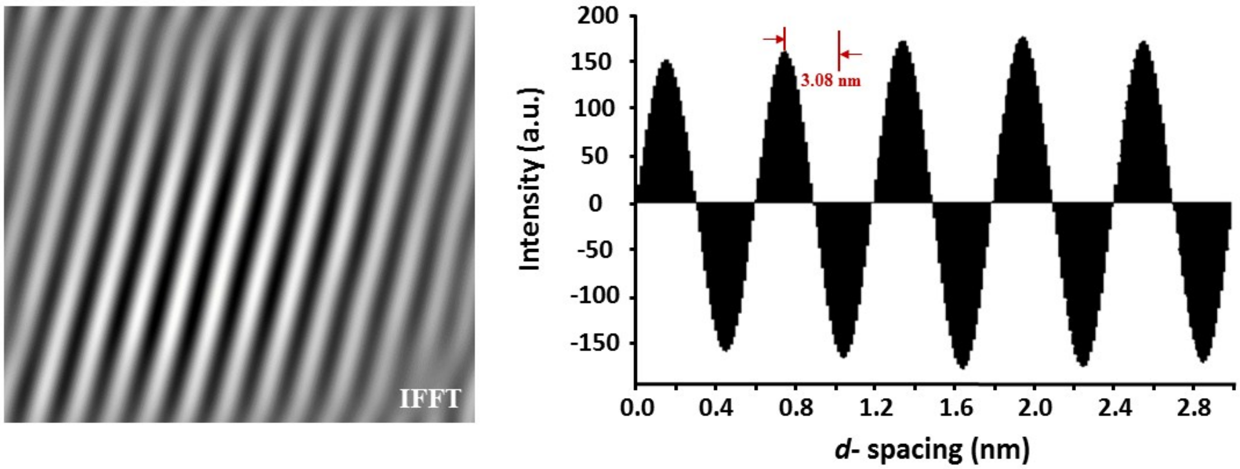

Fig. S10 Inverse fast Fourier transformation and related *d*-spacing.

XRD (1/3)

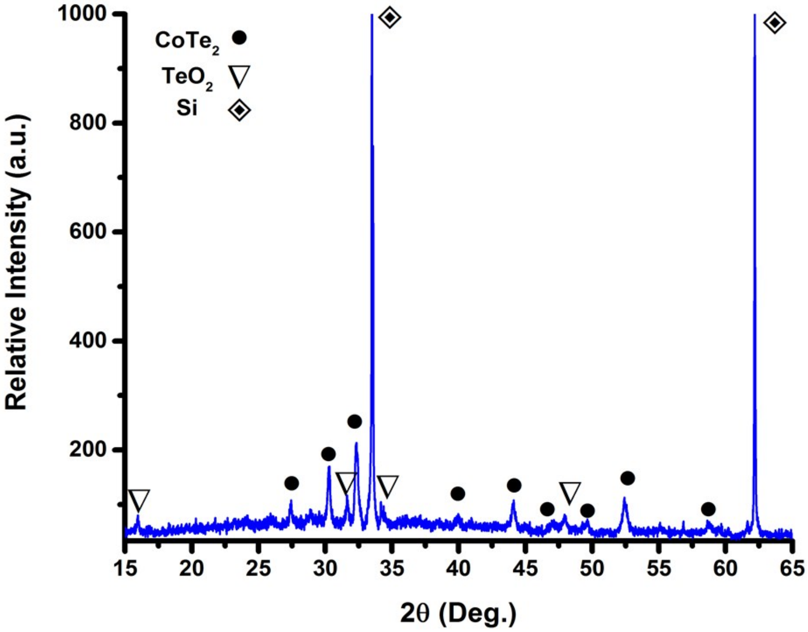

Fig. S11 XRD of the excess-volume coated sample on Si-MQs using the drop-casting method.

The excess volume (>100 μL) coated sample was also measured by XRD to further confirm the successful formation of the $CoTe_2$ product at the surface (Fig. S12). Some other peaks with low intensity could be related to TeO_2 formed on the surface because of the low resistance of $CoTe_2$.[2] We also demonstrated the XRD results of the final product through 30 μL volume drop-casting, which showed no evidence of the presence of an initial Na_2TeO_3 compound in the final product through the cation-exchange reaction (Fig. S13). The excess volume coated sample (>100 μL) was made so that the peak position of the final product was detectable with a higher relative intensity across the microwire array. As shown in this Fig., the majority of the sample included single crystalline silicon microwires and $CoTe_2$ decorated between and across the array. A low amount of TeO_2 (*JCPDS N.O 8-0484*) was observed, which could be attributed to the low oxidation resistance of $CoTe_2$.[2]

XRD (2/3)

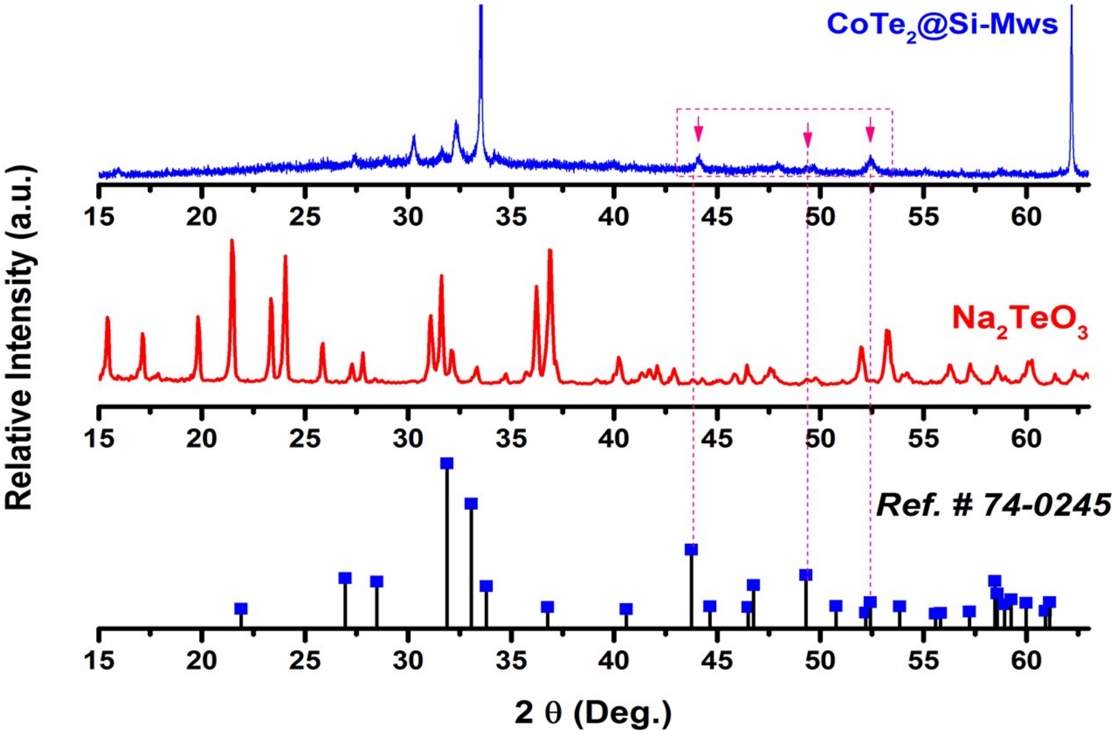

Fig. S12 XRD of the excess volume coated sample compared with Na_2TeO_3.

Fig. S13 (red spectra) shows the XRD results from the excess volume coated sample on the Si-MWs compared with Na_2TeO_3 as one of the starting materials. As shown in this Fig., the sharp peaks from sodium tellurite in the range of 2θ = 15–30° and 35–40° were not present in the final product. Although a slight similarity between some peaks may be found from the raw material and the product, the three characteristic peaks at 43.7°, 49.3°, and 52.4° confirmed the $CoTe_2$ formation across the Si-MQ assembly. This result also indicated the formation of the new crystallite through the cation exchange reaction.

X-ray photoelectron spectroscopy (XPS) (3/3)

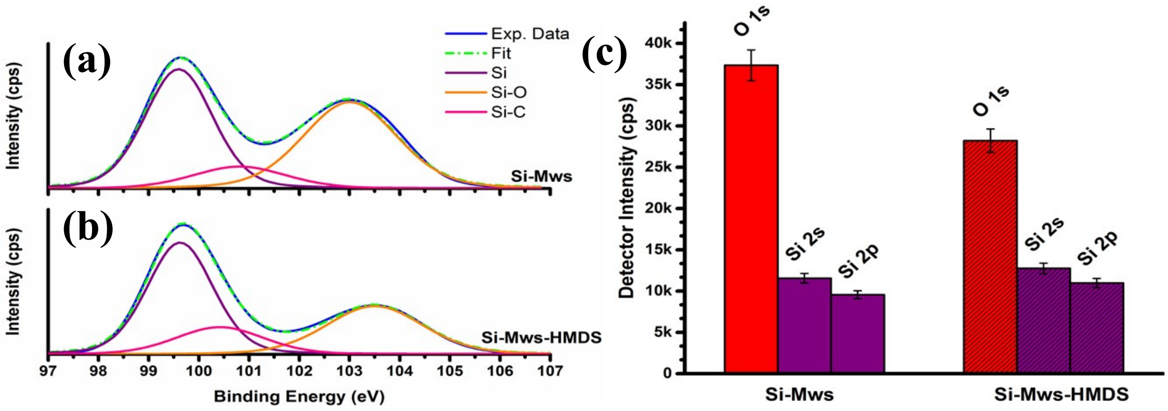

Fig. S13 XPS spectra of the (a) pristine Si-MW array, (b) vapor-treated Si-MW surface HMDS, and (c) bar diagram of (a) and (b) related to the area behind the curve.

The Si 2p region of the pristine Si-MW- and Si-MW-HMDS-treated samples was analyzed in Fig. S16a considering spin-orbital splitting. The spectra deconvoluted with 80% Gaussian–20% Lorentzian peak fitting. The peak centered at 103.5 eV was related to SiO_2. Elemental Si appeared at 99.4 eV[3]. The peak positioned at 101–101.5 eV was related to the Si–C bond and intermediate oxide states. As indicated in Fig. S16b, the Si–O area decreased for the HMDS-treated samples, thereby confirming the HMDS role in preventing more silicon surface oxidation for the purpose of preserving morphology. Fig. S16c demonstrates a bar diagram of the surface area extracted from the survey spectrum for both samples. Analysis of the oxygen and silicon ratio in the Si-MW samples treated by HMDS vapor revealed a lower oxygen content presence on the surface, which pointed out the HMDS role in preserving the silicon wafer surface from water adsorption and more silicon oxidation, thereby preserving sample morphology.[4]

UV–Vis spectroscopy and LSV (1/1)

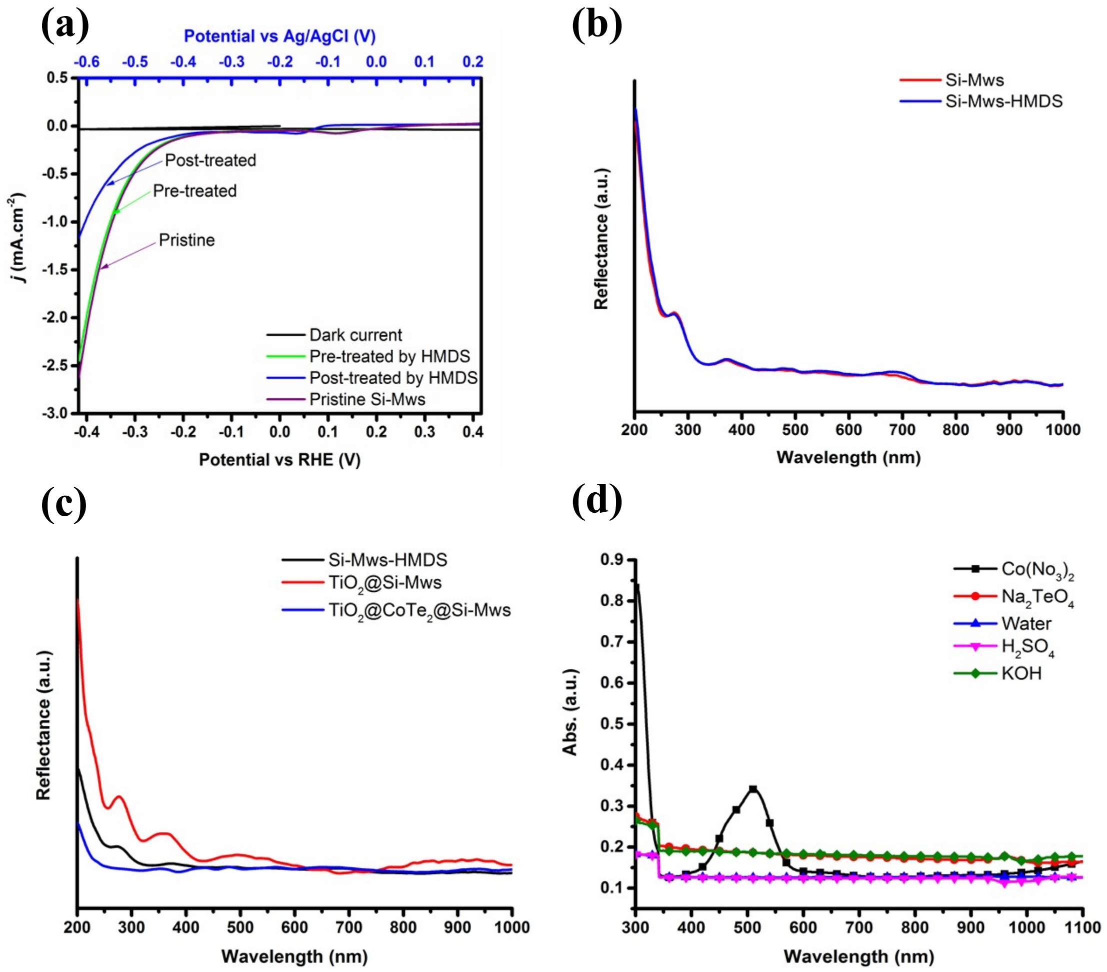

Fig. S14 (a) LSV measurement of the Si-MW treated by HMDS vapor without *iR* compensation vs nominal RHE. (b) Reflectance spectrum of the pristine Si-MW treated by HMDS vapor. (c) Reflectance spectrum of the 10 nm ALD–TiO_2 coated $CoTe_2$ at Si-MWs compared to the HMDS vapor treated Si-MW array and TiO_2-coated Si-MWs. (d) Absorbance of the solutions, where $CoTe_2$ at the Si-MW samples were immersed for over 24 h at room temperature.

Fig. S19a shows the LSV measurement of the bare Si-MWs treated with 100 μL HMDS vapor for 5 min at 100 °C before (pre-treatment) and after (post-treatment) furnace. The pre-treated silicon wafer had a similar trend to the bare silicon. Post-treating the wafer would decrease the current density to -1.2 $mA \cdot cm^{-2}$ because of an excess amount of HMDS on the surface, which impeded water reduction at the electrode interface with electrolyte because of the hydrophobic character of the HMDS. No particle formation was observed on the surface because of hydrolysis. Treatment was applied only to increase the stability of the $CoTe_2$ particles coated on the surface. In Fig. S19b, the reflectance spectra demonstrated absorbance in the visible and near infrared region (400–1000 nm) for the Si-MW-HMDS with no change observed after the HMDS treatment. All peaks around 375, 270, and 205 nm were related to the silicon microwire array.[5] The reflectance spectra of $CoTe_2$@TiO_2-Si-MWs showed full coverage over the visible spectrum by some absorbance peaks in the UV region related to the TiO_2 coating. The same trend was also observed for ALD-10 nm TiO_2 at Si-MWs with decrease in the core silicon absorbance because of the TiO_2 deposition in the shorter wavelength (<400 nm). Fig. 19c shows that the amorphous TiO_2 had no absorbance in this region and only applied for protecting the silicon cores from further oxidation during the PEC and acting as a passivation layer. The peaks almost disappeared for $CoTe_2$@TiO_2-Si-MWs, thereby revealing an optimized absorbance among other compositions. The HER catalyst systems may be inactive or unstable in strong basic electrolytes. Therefore, the samples were tested in the basic solution as well as in acidic and neutral solutions. The stability of $CoTe_2$@Si-MWs was evaluated by the UV–Vis spectra of the immersed samples in water (pH = 6.8), H_2SO_4 (1 M), and KOH (1 M) for 24 h compared with the distinct absorbance of $Co(NO_3)_2$ (100 ppm) centered around 500 nm (Fig. 19d). No sample revealed a peak in the 500 nm wavelength, which confirmed that no Co^{2+} adsorbed on the surface. Furthermore, the stability of the coated sample on the silicon wafer to be decomposed was observed. Potential conversion to nominal RHE follow by theoretical equation (1):

$$E_{RHE}\ (V) = E_{Ag/AgCl}\ (V) + (0.0591 \times pH) \qquad (1)$$

Photoelectrochemical measurements (PEC) (1/5)

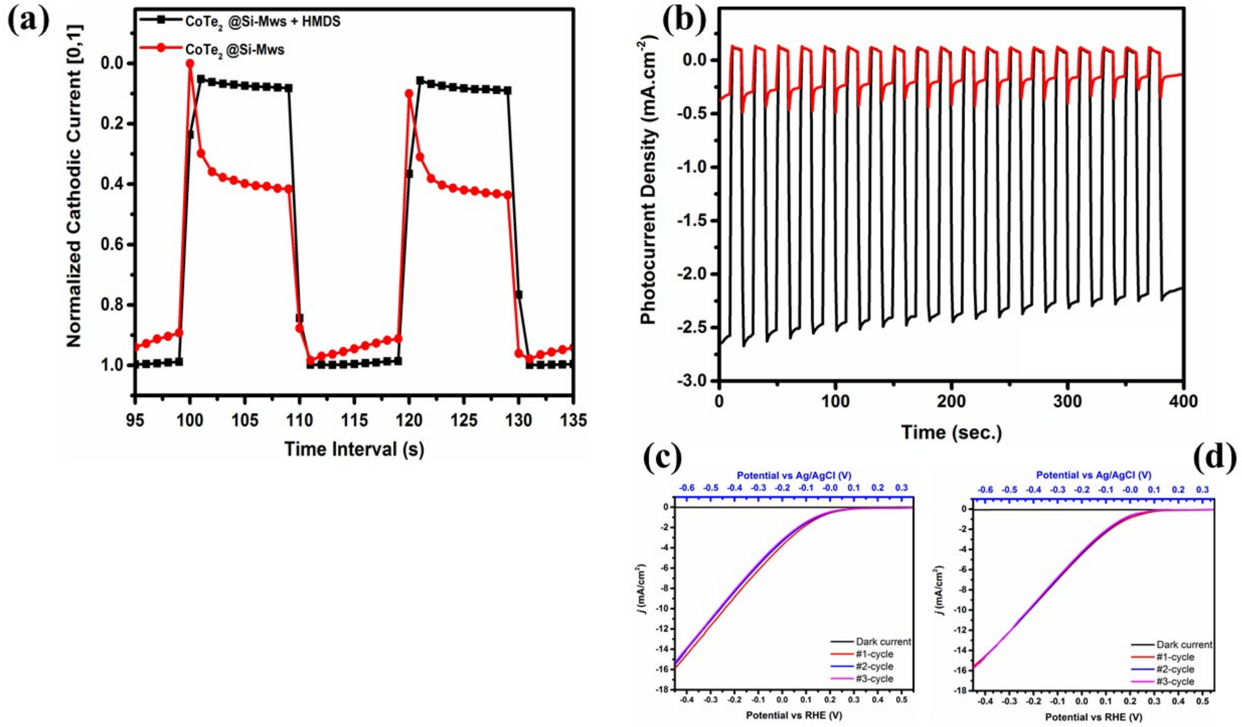

Fig. S15 (a) Normalized cathodic current of $CoTe_2$ at the Si-MWs at 0 V vs. the RHE under chopped illumination. (b) Relative photocurrent transient measurement by chronoamperometry. (c) Untreated and (d) vapor-treated samples by 100 μL HMDS at ~100 °C for 5 min without *iR* compensation vs nominal RHE.

Accordingly, 10 μL of the drop-casting solution was coated on the Si-MWs. As shown in Fig. S20 (a, b), the sample without HMDS demonstrated an overshoot photocurrent spike, which was consistent with the photogenerated carrier transport process limited by the recombination in the bulk or grain boundary. By applying HMDS vapor coating, the accumulated photogenerated electrons at the semiconductor–liquid junction (SCLJ) no longer limited the charge carrier transport. The sample without HMDS did not exhibit a stable current as treated sample in different cycles (totally 3 cycles) in LSV measurement (c, d). These results indicated that the photo-generated charge carriers accumulated on the surface, mostly because of loose binding to the Si-

MWs, hindered to migrate to the SCLJ, and interrupted reaching the photocurrent with the steady state at 0 V vs. RHE.

PEC (2/5)

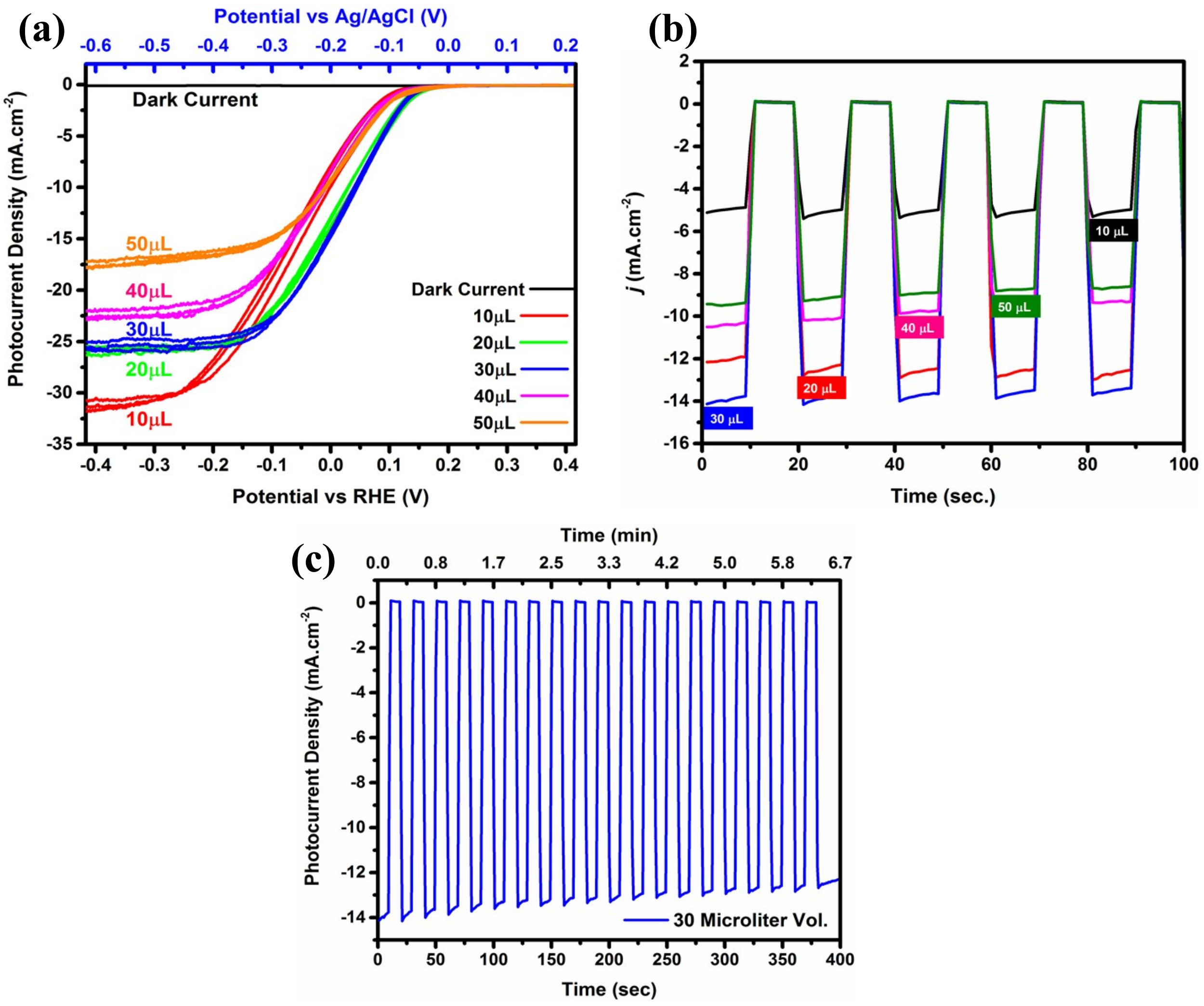

Fig. S16 (a) LSV measurement of the Si-MW samples coated with various drop-casting volumes and annealed at 400 °C without *iR* compensation vs nominal RHE.. (b) Corresponding photocurrent transient at 0 V vs RHE at 25 °C after three cycles of LSV measurement. (c) Photocurrent transient of the optimum sample onto the silicon microwire.

A different volume of the drop-casting solution was studied to optimize the drop-casting volume and achieve the highest photocurrent density. As demonstrated in Fig. S21a, three LSV cycles were conducted in the range of +0.5 to -0.45 vs. RHE on the coated Si-MWs treated with HMDS vapor with the $CoTe_2$ particles decorated across the wire array. The LSV measurement of the various amounts of the cocatalyst was conducted through scanning potential in the range of +0.45

to -0.5 V vs. RHE at 25 °C in H_2SO_4 0.5M (pH = 0.3). All samples had almost consistent onset potential (±0.02 V) and current density (±0.03 $mA\cdot cm^{-2}$) through three cycles. Fig. S21b shows the transient photocurrent density under copped illumination (100 $mW\cdot cm^{-2}$) for samples with different volume coatings on the surface at 0 V vs. RHE. All samples demonstrated almost an exact current density measured at 0 V vs. RHE in the LSV measurement. No overshoot or spike peaks were observed for the measured sample, which confirmed that there were no defect sites for the photogenerated carrier recombination. The reducing trend by increasing the cocatalyst on the silicon wafer was attributed to the reduced light absorption in the formed layer on the surface by the agglomerated cocatalyst particles. Fig. S22 shows the comparison of the TiO_2-coated electrode with other samples and different drop-casting volumes.

PEC (3/5)

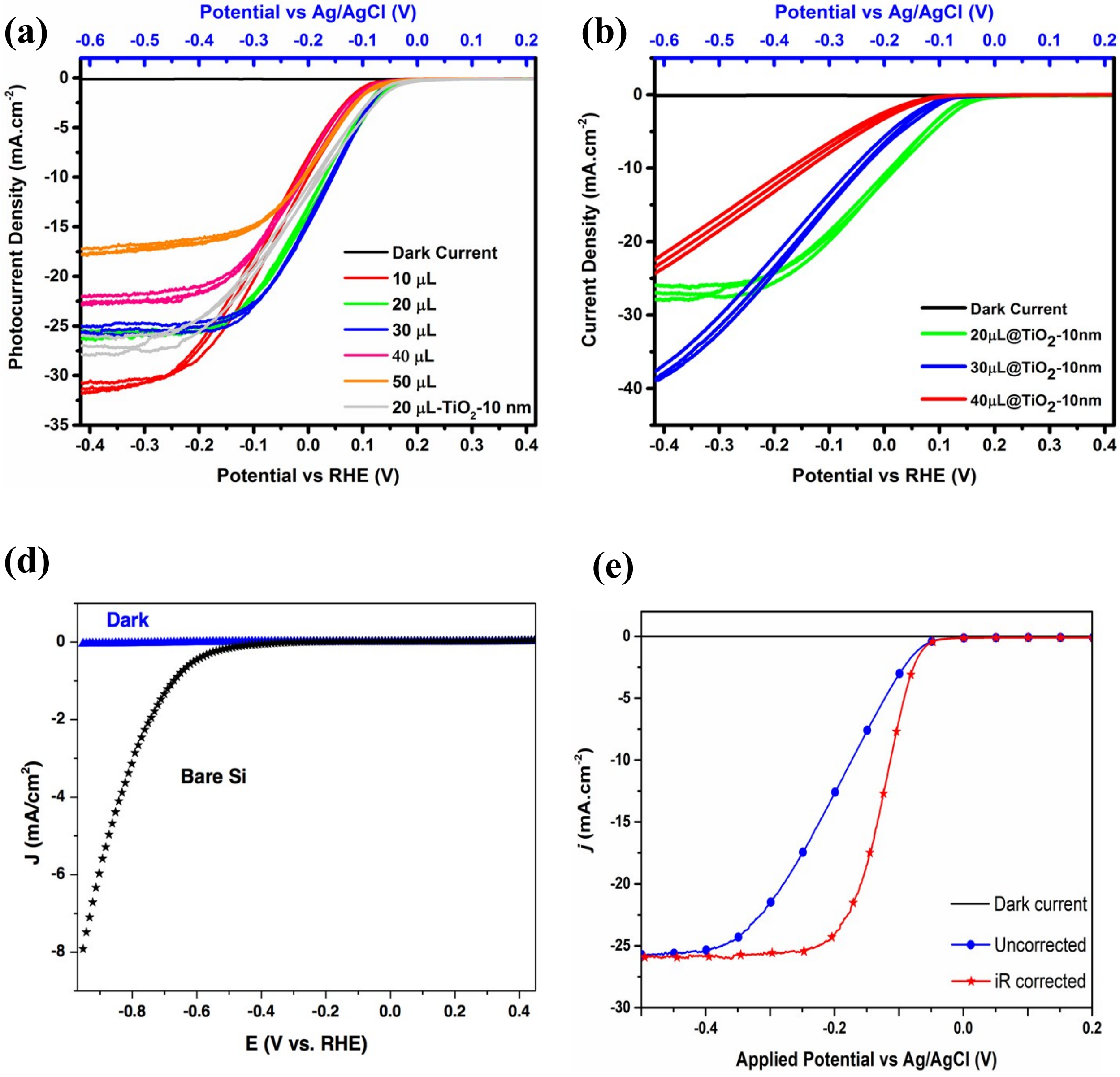

Fig. S17 LSV measurement without *iR* compensation vs nominal RHE at 25 °C for different drop-casting volumes of (a) Si-MWs and (b) ALD-TiO$_2$-10 nm at Si-MWs. (d) Bare Si-MWs with onset potential of -0.49 V vs RHE. (e) *iR* correction in LSV measurement with R_s= 6 ohm.cm^{-2} calculated from EIS data.

PEC (4/5)

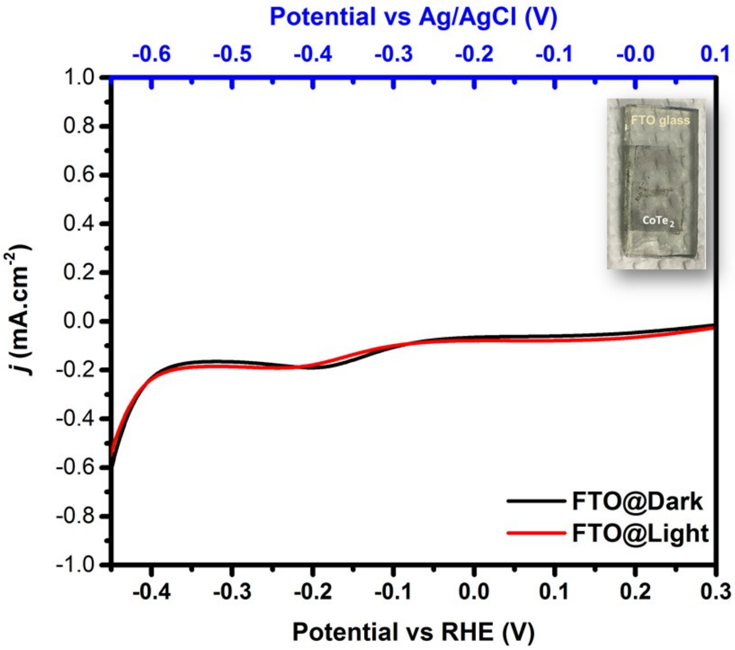

Fig. S18 LSV measurement without *iR* compensation vs nominal RHE of $CoTe_2$ coated on the FTO glass with the same drop-casting procedures. The inset shows a photograph of $CoTe_2$ at the FTO.

CoTe2@FTO preparation Fluorine tin oxide (FTO) glass substrate (17 Ω square-1) was cleaned by a series of sonication in 3% soap/DI water, acetone, and ethanol (each solution for 15 min), then rinsed several times with DI water, and finally sonicated in 2-propanol (15 min). The similar drop-casting method was used for face-up conducting layer of the FTO for the photoactivity measurement.

$CoTe_2$@FTO glass exhibited no shift in the onset potential and no photoactivity of the $CoTe_2$ sample under illumination (100 $mW\cdot cm^{-2}$), confirming the half-metallic nature of $CoTe_2$ underlying 30 μL of the coated sample on the FTO glass fabricated using the same procedure.

PEC (5/5)

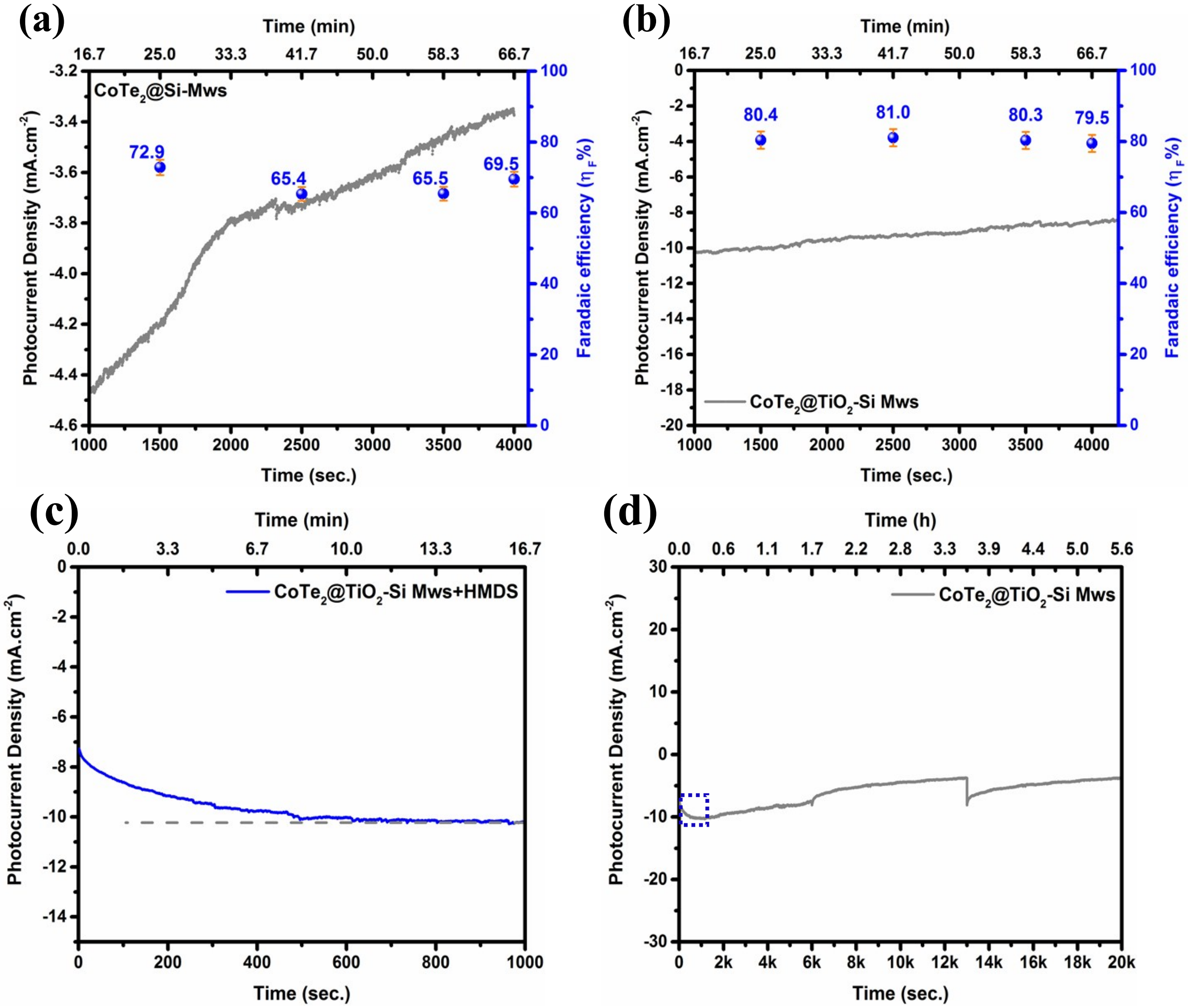

Fig. S19 Chronoamperometry measurement and corresponding Faradaic efficiency of (a) $CoTe_2$ at Si-MWs and (b) $CoTe_2$ at ALD-10nm–TiO_2–Si-MWs at constant 0 V potential vs RHE under AM.15 G irradiation; (c) initial 1000 s. and (d) PEC measurement for more than 5 h. Selected area shows initial 15 minutes.

References:

1 R. Shi, X. Liu, Y. Shi, R. Ma, B. Jia, H. Zhang and G. Qiu, *J. Mater. Chem.*, 2010, **20**, 7634.

2 K. Wang, Z. Ye, C. Liu, D. Xi, C. Zhou, Z. Shi, H. Xia, G. Liu and G. Qiao, *ACS Appl. Mater. Interfaces*, 2016, **8**, 2910–2916.

3 H. Watanabe and T. Hosoi, in *Physics and Technology of Silicon Carbide Devices*, 2012, pp. 235–250.

4 L. Zhang, C. Liu, A. B. Wong, J. Resasco and P. Yang, *Nano Res.*, 2015, **8**, 281–287.

5 C. J. Chen, M. G. Chen, C. K. Chen, P. C. Wu, P. T. Chen, M. Basu, S. F. Hu, D. P. Tsai and R. S. Liu, *Chem. Commun. (Camb).*, 2015, **51**, 549–52.